Phase-resolved emission spectroscopy of a hydrogen rf discharge for the determination of quenching coefficients

T. Gans,* Chun C. Lin,† V. Schulz–von der Gathen, and H. F. Döbele
Universität Essen, Institut für Laser- und Plasmaphysik, 45117 Essen, Germany
(Received 2 August 2002; published 28 January 2003)

Collisional effects can have strong influences on the population densities of excited states in gas discharges at elevated pressure. The knowledge of the pertinent collisional coefficient describing the depopulation of a specific level (quenching coefficient) is, therefore, important for plasma diagnostics and simulations. Phase-resolved optical emission spectroscopy (PROES) applied to a capacitively coupled rf discharge excited with a frequency of 13.56 MHz in hydrogen allows the measurement of quenching coefficients for emitting states of various species, particularly of noble gases, with molecular hydrogen as a collision partner. Quenching coefficients can be determined subsequent to electron-impact excitation during the short field reversal phase within the sheath region from the time behavior of the fluorescence. The PROES technique based on electron-impact excitation is not limited—in contrast to laser techniques—by optical selection rules and the energy gap between the ground state and the upper level of the observed transition. Measurements of quenching coefficients and natural fluorescence lifetimes are presented for several helium ($3\,^1S$,$4\,^1S$,$3\,^3S$,$3\,^3P$,$4\,^3S$), neon ($2p_1$,$2p_2$,$2p_4$,$2p_6$), argon ($3d_2$,$3d_4$,$3d_1'$ and $3d_3$), and krypton ($2p_1$,$2p_5$) states as well as for some states of the triplet system of molecular hydrogen.

DOI: 10.1103/PhysRevA.67.012707 PACS number(s): 34.80.My, 33.50.Hv, 34.80.Dp, 52.70.Kz

I. INTRODUCTION

Low-density plasmas are often characterized by the so-called corona equilibrium, in which excitation takes place by collisions, predominantly from the ground state, whereas deexcitation is exclusively by radiative transitions. Spectroscopic techniques allow under these conditions to draw conclusions with respect to various plasma parameters (e.g., particle temperatures [1], densities [2], and electron energy distributions [3]), if the necessary data basis is available. This concept is, however, of rather limited applicability for processing plasmas, since already at gas pressures exceeding 10 Pa, quenching can have a pronounced influence on the population densities of excited states. The knowledge of quenching coefficients is, therefore, essential for the correct interpretation of experimental data for plasma diagnostics based on optical emission spectroscopy [4] and also laser induced fluorescence spectroscopy, with one- or two-photon excitation [5,6], since the measured spontaneous emission intensities, from which the population densities of excited states i are inferred, are influenced by the effective decay rate A_i that is affected by quenching in the following manner:

$$A_i = \sum_k A_{ik} g_{ik} + \sum_q k_q n_q . \tag{1}$$

Here, k_q is the coefficient describing quenching collisions by the species q of density n_q; A_{ik} and g_{ik} are the spontaneous transition rate and the escape factor, respectively.

The coefficients k_q take into account all inelastic collisional processes by the collision partner q of the level i under consideration. (The term ''collisional deexcitation coefficient'' is also in use instead of quenching coefficient, since the effect is indeed a deexcitation in most cases.) The deexcitation consists in an excitation energy transfer from one particle to internal energy of the collision partner and translational energy of both particles. A more detailed description of the deexcitation processes can be found in Refs. [7–13].

Since the deexcitation cross section σ_q is often only weakly temperature dependent [14–16], the following temperature dependence of the collisional deexcitation coefficient k_q results for a thermal distribution of the collisional partner particles (of average thermal velocity $\langle v \rangle$) [17]:

$$k_q(T) = \sigma_q \langle v \rangle = \sigma_q \sqrt{\frac{8 k_B T}{\pi \mu}}. \tag{2}$$

k_B is the Boltzmann constant and μ is the reduced mass of the colliding particles. The knowledge of the temperature T is, therefore, of decisive importance whenever deexcitation coefficients in gas discharges are applied or measured.

Collisional deexcitation coefficients of excited states are usually determined after pulsed excitation by measuring the effective decay rate A_i, including collisional deexcitation, according to

$$n_i \propto \exp(-A_i t). \tag{3}$$

The excitation can be performed, in principle, by laser irradiation with suitable photon energy or by electron collisions. Laser excitation is subject to optical selection rules [18] and has the additional limitation that the photon energy has to bridge the energy gap between the ground and excited states,

*Present address: Institut für Experimentalphysik V, Ruhr-Universität-Bochum, 44780 Bochum, Germany. Electronic address: Timo.Gans@web.de

†Permanent address: Department of Physics, University of Wisconsin, Madison, WI 53706.

which will often be impossible with current tunable laser systems, e.g., excimer pumped frequency-doubled dye lasers emitting down to $\lambda \approx 200$ nm (an energy of about 6.5 eV) even with two-photon excitation.

Quenching coefficients of noble gases are of particular importance, since these are often used as reference gases in plasma diagnostic applications. It is possible for xenon [7,19], krypton [8,19], and argon [20,21] to overcome the pertinent energy gaps by two-photon excitation with uv and vuv lasers (Xe, 8–12 eV; Kr, 10–14 eV; Ar, 12–16 eV). In the cases of neon (17–21 eV) and helium (20–24 eV), however, the energy gaps to the ground states are too large. Optical excitation from metastable states may represent an alternative. This allows self-quenching coefficients to be determined [22]. This method does not allow, however, to measure quenching coefficients for excited states of neon or helium with molecules, e.g., hydrogen, since the population densities of metastable states of noble gases are very low in discharges with molecular components [23]. In this paper, we adopt an alternative approach of using pulsed electron excitation to determine collisional deexcitation coefficients. A special feature of our experiment is the use of a capacitively coupled rf (CCRF) discharge as an intensive, pulsed electron source. The CCRF discharges operating at 13.56 MHz in hydrogen [24–26] exhibit a field reversal phase resulting in a pulse of electrons through the sheath region. A typical pulse has a duration of about 15 ns and decays from the half maximum to zero in less than 3 ns as shown in Ref. [25]. After excitation by the pulsed electron current into the excited level under consideration, the temporal dependence of the fluorescence is monitored. To analyze the observed fluorescence data, we utilize the recently reported electron-impact excitation cross sections of the noble gases measured in an electron beam, apparatus at low pressures. Because of the complexity of the excitation dynamics in a CCRF discharge as compared to the electron beam experiment, we have developed a model to account for the secondary collisional processes in a CCRF discharge that contribute to the population of the excited states. An advantage of using electron-impact excitation over laser excitation is that the former is capable of accessing, in principle, all excited states without restrictions to optical selection rules or excitation energy [27]. However, unlike laser excitation, electron-impact excitation produces atoms in numerous high-lying excited levels, so that the population of the excited state under consideration by cascade from the higher levels must be taken into consideration. In this paper, we show how one can apply the electron-impact cross sections (from electron-beam experiments) to the CCRF discharges in order to determine the quenching coefficients from the temporal fluorescence measurements. The CCRF discharge is operated with hydrogen gas, a direct application is to study quenching of excited states of H_2 by ground-state hydrogen molecules. By adding a small amount of noble gases to the discharge, we have also measured the coefficients of quenching various excited states of the noble gases by H_2 molecules.

II. EXPERIMENT

The measurements are performed in an asymmetric (one electrode grounded) CCRF discharge at 13.56 MHz in hydrogen with small admixtures of noble gases. The setup is described in detail elsewhere [1]. The flat cooled stainless-steel electrodes, 100 mm in diameter, are 25 mm apart. The gas pressure ranges between 20 Pa and 400 Pa; the rf power for these experiments is 100 W. Gas flow and gas mixture are adjusted by mass flow controllers. The discharge axis is imaged onto the entrance slit of a 2 m spectrograph (Jenoptik PGS 2, 1302 mm^{-1} grating), see Fig. 1. A fast gated intensified charge coupled device camera (Picostar, LaVision GmbH, 576×384 pixels, 13.2×8.8 mm^2) samples spectral intervals of about 4.5 nm with a spectral resolution of 0.03 nm and a spatial resolution of about 0.5 mm by averaging over several pixels. This spectral resolution allows us to separate the observed emission lines from numerous molecular emission lines in the hydrogen discharge. Phase-resolved measurements are possible by locking the gate to a definite phase position within the rf cycle. The intensities measured in the gate time of 3 ns can be integrated over many rf cycles for this phase setting. A variable delay between a fixed phase and the gate allows one to cover the complete rf cycle.

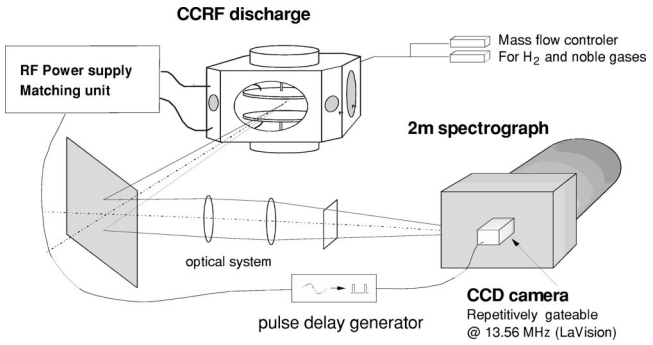

FIG. 1. Experimental setup of the discharge chamber and the electronic and optical components for phase-resolved optical emission spectroscopy (PROES).

III. MODELING OF EXCITED-STATE POPULATION DYNAMICS DURING THE DISCHARGE CYCLE

The CCRF hydrogen discharge is characterized by several particularities regarding the excitation processes and the resulting optical emission. Understanding the excitation dynamics [24,25] in the discharge is essential for the measurement of quenching coefficients by phase-resolved optical emission spectroscopy (PROES). Figure 2 displays the space-time evolution of the H_α-line emission. The abscissa comprises of two rf periods, 74 ns each. The transverse axis indicates the distance from the powered electrode located at the bottom of the figure. Several emission structures (I–IV) can be distinguished. Structures I and II can be explained on the basis of *E*-field measurements [25]. Structure I is caused by a field reversal across the space-charge sheath—typical for hydrogen rf discharges. It is explained by the relatively large mobility of the ions and relatively small mobility of the electrons in this discharge [26]. Electrons are accelerated towards the powered electrode inducing strong impact excitation. This excitation in front of the electrode is exploited for the measurement of quenching coefficients, since, when the

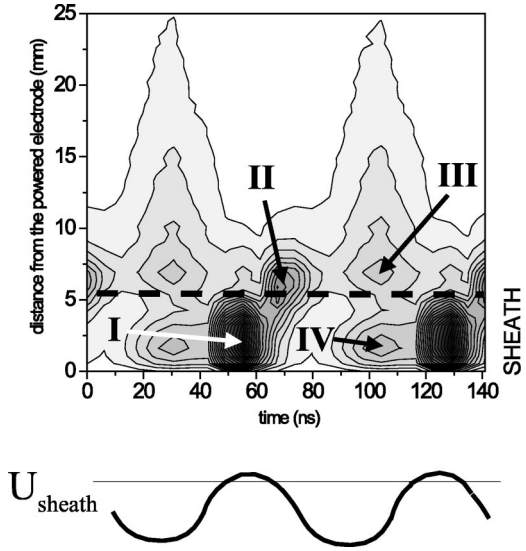

FIG. 2. Space and time resolved emission of H_α from the CCRF hydrogen discharge operating at 141 Pa and 100 W (U_{pp} = 750 V). Also shown is a sketch of the sheath voltage as measured by Czarnetzki *et al.* [25]

sheath potential becomes negative again, electrons are pushed out of the sheath towards the plasma bulk. Note that there is no electron-impact excitation for the rest of the rf cycle in front of the powered electrode. The characteristic decay rate of the subsequent fluorescence is influenced by quenching. It allows us, therefore, to infer the pertinent coefficient. Structure II is related to the sheath expansion heating of the electrons moving to the plasma bulk. Structure III results from fast secondary electrons created by ion impact, whereas structure IV is related to fast hydrogen atoms created at the electrode surface by the impact of hydrogen ions. These fast hydrogen atoms can excite the background gas by heavy-particle collisions. Due to the small mass of hydrogen ions they are able to follow the applied electric field with only a short delay [24]. Thus, this time-dependent ion bombardment of the electrode determines the time dependence of secondary electrons and fast hydrogen atoms related to structure III and structure IV, respectively.

The determination of the effective decay rates after the strong excitation by electron collisions during the field reversal phase requires to take into account also the influence of excitations by heavy-particle collisions and by cascading processes from higher electronic states. This can be done on the basis of a time-dependent model for the population density, which is explained in the following.

A. Heavy-particle collisions and cascade processes

Cascade transitions from higher levels are often small in comparison to the collisional excitation of the radiating level. The situation is then considerably simplified. We consider the Kr $2p_2$ line as an example of these conditions [28]. Figure 3 shows one period of the phase-resolved emission in front of the powered electrode. The zero of the time scale was chosen to be at the end of the electronic collisional excitation. After the strong electron-impact excitation due to

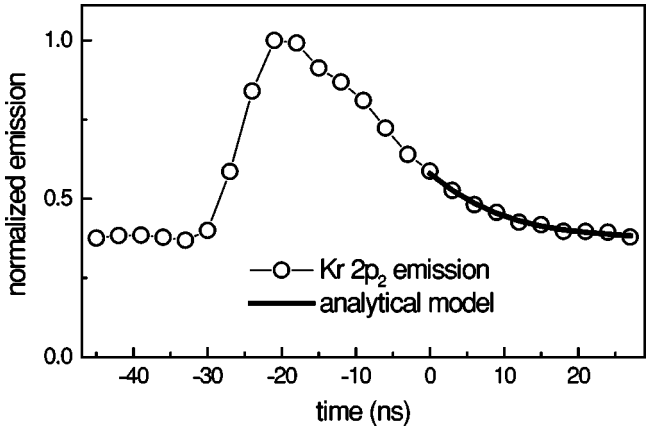

FIG. 3. Phase-resolved emission in front of the powered electrode of the Kr $2p_2$ line.

the field reversal, the fluorescence decay influenced by quenching with molecular hydrogen can be observed. With the known [19] quenching coefficient and natural lifetime of the Kr $2p_2$ line, the excitation function $E_i(t)$ of the observed level i can be calculated from the emission (proportional to the population density n_i) in the following manner:

$$n_0 E_i(t) = \frac{dn_i(t)}{dt} + A_i n_i(t). \tag{4}$$

The excitation out of the ground state is proportional to both the ground-state density n_0 and the excitation function $E_i(t)$. The term ''excitation function'' is sometimes used differently in the literature. We will, however, use the definition given above throughout the paper. The excitation function in Fig. 4 exhibits a weak contribution related to heavy particle collisions of fast hydrogen atoms (max. at $\approx$30 ns), after a strong excitation due to the field reversal (max. at ≈ -25 ns) and a weak excitation due to the sheath expansion (max. at ≈ -10 ns). The time behavior of the density of energetic atoms corresponds to that of the ions, since they are generated at the driven electrode by ion bombardment. The hydrogen ions are able to follow the applied rf voltage

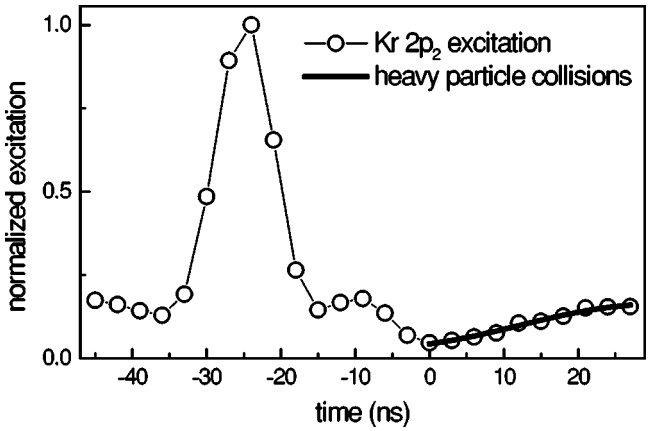

FIG. 4. Excitation function of the Kr $2p_2$ level in front of the powered electrode.

with only a small delay because of their relatively small inertia. The time dependence of the excitation by heavy-particle collisions

$$\mathrm{H}_{fast}+X\rightarrow\mathrm{H}_{fast}+X^{*} \tag{5}$$

(where X represents the observed species) can, therefore, be described by a sinusoidal function including the aforementioned delay with respect to the applied voltage. The excitation function $E_i(t)$ of the level under consideration can, therefore, be separated in the following manner:

$$E_i(t)=E_i^e(t)+\frac{E_i^H}{2}\left[1+\cos\left((t-t_{heavy})\frac{2\pi}{T_{rf}}\right)\right]. \tag{6}$$

$E_i^e(t)$ describes the excitation by electron collisions and $E_i^H(t)$ that by collisions with energetic hydrogen atoms. T_{rf} is the rf period. The time of maximum excitation by heavy particle collisions t_{heavy} can easily be inferred from the excitation function of atomic hydrogen since this mechanism has a strong influence on the latter. The temporal behavior described by Eq. (6) is represented for $t>0$—i.e., after the electronic excitation—in Fig. 4, together with the measured excitation function. It is obvious that the time characterisitic of the heavy-particle collisional excitation is well reproduced.

In contrast to the Kr $2p_2$ level discussed above, cascading effects can be, however, of great importance for the population of other levels. Including these effects out of a level c leads to an additional population term in the rate equation for the density n_i of an excited level i, so that the following equation results:

$$\frac{dn_i(t)}{dt}=n_0E_i(t)-A_in_i(t)+A_{ci}n_c(t). \tag{7}$$

n_c is the population density of the upper (cascading) level and A_{ci} is the pertinent transition rate into the level under consideration. The meaning of the other quantities are the same as above for the case without cascading contributions [Eq. (4)].

The population density n_c obeys the following rate equation:

$$\frac{dn_c(t)}{dt}=n_0E_c(t)-A_cn_c(t). \tag{8}$$

The designation of the quantities in this expression is analogous to Eq. (4). The coupled differential equations for the level under consideration [Eq. (7)] and the cascade level [Eq. (8)] can be solved, in a general manner, for the periodic boundary conditions of the present rf discharge.

We will discuss in the following a more intuitive approach with respect to the determination of quenching coefficients.

B. Deexcitation processes

A detailed knowledge of the temporal behavior of the electronic excitation is not necessary for the determination of the effective decay rate since only the population history after the excitation matters. The only basic information required is that no further electronic excitation will take place after the sheath expansion. This is why $t=0$ is chosen at the end of the electronic excitation, which is at the same time the beginning of the interval, during which the effective deexcitation can be determined. The onset of the electronic excitation is, therefore, at $t=-t_0$.

For the time interval under consideration $0<t<T_{rf}-t_0$, we find for the excitation function described by Eq. (6), the following behavior of the population density $n_i(t)$ by solving the system of Eqs. (7) and (8):

$$\begin{aligned}n_i(t)=&\frac{n_0\widetilde{E_i^e}(0,A_i)}{1-e^{-A_iT_{rf}}}e^{-A_it}+\frac{A_{ci}}{A_i-A_c}\left[\frac{n_0\widetilde{E_c^e}(0,A_c)}{1-e^{-A_cT_{rf}}}e^{-A_ct}-\frac{n_0\widetilde{E_c^e}(0,A_i)}{1-e^{-A_iT_{rf}}}e^{-A_it}\right]\\&+\frac{n_0E_i^H}{2A_i}\left\{1+\left[1+\left(\frac{2\pi}{A_iT_{rf}}\right)^2\right]^{-1/2}\sin\left((t-t_{heavy})\frac{2\pi}{T_{rf}}+\phi_i(A_i)\right)\right\}\\&+\frac{n_0E_c^HA_{ci}}{2A_iA_c}\left(1+\left\{\left[1+\left(\frac{2\pi}{A_iT_{rf}}\right)^2\right]\left[1+\left(\frac{2\pi}{A_cT_{rf}}\right)^2\right]\right\}^{-1/2}\sin\left((t-t_{heavy})\frac{2\pi}{T_{rf}}+\phi_{ci}(A_c,A_i)\right)\right).\end{aligned} \tag{9}$$

E_x^H stands for the excitation amplitude of the level x by collisions with fast hydrogen atoms, A_y is the effective deexcitation rate for the level y, and both the levels x and y cover the fluorescence level i and the cascading level c. $n_0\widetilde{E_x^e}(0,A_y)$ is the population of the state x—depending on A_y—which has been accumulated during the cycle by electronic collisions out of the ground state until the time $t=0$ with

$$\widetilde{E^e}_x(0,A_y)=\int_{-t_0}^{0}E_x^e(t')\exp(A_yt')dt'. \tag{10}$$

The following abbreviations have been used in addition:

$$\phi_i=\arctan\left(\frac{A_iT_{rf}}{2\pi}\right), \tag{11}$$

$$\phi_{ci} = \arctan\left(\frac{T_{rF}}{2\pi\left(\frac{1}{A_i}+\frac{1}{A_c}\right)} - \frac{2\pi}{T_{rf}(A_i+A_c)} \right). \quad (12)$$

The first term of Eq. (9) describes the purely exponential decay without heavy-particle collisions and cascade processes. This is the leading term in view of the comparatively weak heavy-particle excitation and often small cascading contribution. The initial value of the exponential decay is proportional to the ground-state density n_0 and the amplitude of the electronic excitation. The denominator is determined by the rf period and describes, as a function of the effective deexcitation rate A_i, the amount of population that is saved for the next rf cycle. The following term takes account of the population by cascading out of higher states that are, in turn, also populated by electronic collisions. The influence of heavy-particle excitations is described by the third term. The periodicity leads to a contribution constant in time in addition to the sinusoidal dependence. The latter is phase shifted relative to the sine of the excitation as a consequence of the finite decay rate of the level under consideration. The last term describes cascade processes as a consequence of heavy-particle excitation of the upper cascading level. This term is in fact a second-order correction because of the comparatively weak heavy-particle excitation (see Fig. 4) and often small cascading contribution. The effective deexcitation rates of both levels influence both the phase shift and the ratio of the constant and modulated contributions.

The relations between the population of the cascade level and the level under consideration have to be established in order to take into account the cascade processes in the second term of Eq. (9). This makes it necessary to express $\widetilde{E^e}_c(0,A_i)$ and $\widetilde{E^e}_c(0,A_c)$ in terms of $\widetilde{E^e}_i(0,A_i)$. Optical measurements of electron impact excitation cross sections in electron-beam experiments yield the necessary link. Cascade populations are important in these experiments that have led to detailed measurements of their influence [29–33]. It is necessary, however, to convert the cascade contributions determined for the optically thin case of continuous beam excitations at low particle densities to the present time-dependent situation, which is characterized by comparatively high particle densities and optical thickness for transitions to the ground state.

For the stationary case of the beam experiments (EB), i.e., for monoenergetic electrons, the rate equations yield for the ratio $(C/D)_{EB}$ of the populations by cascade processes and direct excitation for the cascade level c and the level under consideration i the following expression:

$$\left(\frac{C}{D}\right)_{EB} = \frac{\sigma_c}{\sigma_i}\frac{A_{ci}}{A_c^{EB}}. \quad (13)$$

$\sigma_{c,i}$ are the excitation cross sections at the electron-beam energy. Equation (13) shows that the cascade contribution depends on the effective deexcitation rate of the cascade level, and, therefore, on the experimental conditions.

In the plasma case, however, the excitation functions for electronic collisions $E^e_{i,c}(t)$ of the cascade level c and the level i, respectively, have to be taken into account. Their ratio can be expressed by the electron-impact excitation cross sections $\sigma_{i,c}(E)$ at an effective energy E_{eff}, in view of their identical time dependencies:

$$\frac{E^e_c(t)}{E^e_i(t)} = \frac{\int_0^\infty \sigma_c(E)\sqrt{\frac{2E}{m_e}}F(E,t)dt}{\int_0^\infty \sigma_i(E)\sqrt{\frac{2E}{m_e}}F(E,t)dt} = \frac{\sigma_c[E_{eff}(t)]}{\sigma_i[E_{eff}(t)]}. \quad (14)$$

F is the electron energy distribution function. Since the energy dependencies of both levels are similar in the situation considered in this work [29–33], the ratio will exhibit only a weak energy dependence, so that a time-independent approximate value for E_{eff} is sufficient.

Equations (13) and (14) allow us to express the relation between $\widetilde{E^e_c}(0,A_i)$ and $\widetilde{E^e_i}(0,A_i)$ [second term of the second line in Eq. (9)] by the cascade contribution found in electron-beam experiments:

$$\frac{A_{ci}\widetilde{E^e_c}(0,A_i)}{\widetilde{E^e_i}(0,A_i)} = \frac{A_{ci}\sigma_c(E_{eff})}{\sigma_i(E_{eff})} = \left(\frac{C}{D}\right)_{EB} A_c^{EB}. \quad (15)$$

The comparison of the first term of the second line in Eq. (9) with the population of the observed level can also be performed on the basis of Eqs. (13) and (14). The relation is somewhat more complicated in view of the different effective deexcitation rates A_i and A_c,

$$\frac{A_{ci}\widetilde{E^e_c}(0,A_c)}{\widetilde{E^e_i}(0,A_i)} = \left(\frac{C}{D}\right)_{EB} A_c^{EB}\frac{\int_{-t_0}^0 E^e_i(t')e^{A_c t'}dt'}{\int_{-t_0}^0 E^e_i(t')e^{A_i t'}dt'} =: \left(\frac{C}{D}\right)_{EB} A_c^{EB} R(A_i,A_c). \quad (16)$$

The determination of $R(A_i,A_c)$ taking account of the different populations due to different deexcitation rates necessitates an assumption on the time behavior of the excitation function. Figure 4 shows that the excitation by electron collisions in front of the driven electrode between $t=-t_0$ and $t=0$ is characterized by a strong excitation during the field reversal phase and a weak excitation during the sheath expansion phase. The functional dependencies are well described by two triangles with adapted amplitudes and widths. A comparison with approximations by step and δ functions yields differences for $R(A_i,A_c)$ in all investigated cases of

less than 5% so that any important influence on the final deexcitation coefficients can be excluded.

In view of lacking information on the ratio of the excitations by heavy particles, their ratio has been assumed to be the same as for electron-impact collisional excitation:

$$\frac{A_{ci}E_c^H}{E_i^H} := \left(\frac{C}{D}\right)_{EB} A_c^{EB}. \tag{17}$$

In the situation considered in this work, the heavy-particle induced cascading is weak, as mentioned above. No significant differences in the measured quenching coefficients were, therefore, observed between the assumption in Eq. (17) and the two extreme cases of no heavy-particle induced cascading and equal cross sections for heavy-particle collisional excitation of the cascading and the investigated state. The relations (15), (16), and (17) allow us to apply the cascade contributions measured with beam experiments quantitatively to the PROES presented here. This makes it possible to determine effective deexcitation rates and quenching coefficients as will be discussed in more detail in the following.

C. Experimental determination of quenching coefficients

The cascade contribution is calculated, as described in the preceding paragraph, on the basis of electron-beam data in order to obtain the effective deexcitation rate. The time of maximum heavy-particle excitation can be inferred from the excitation function of hydrogen, since it has a strong influence on the latter [24]. The natural lifetimes of the cascade levels—corrected to include reabsorption—can be found in the literature for the levels of interest with exception of krypton. For a specific cascade level, the effective deexcitation rate results for a known density of the collision partner on the basis of a typical deexcitation coefficient. Lacking information on collisional deexcitation coefficients of cascade levels represent a limitation on the method presented here to the cases, where the influence of cascade populations is smaller than the pure exponential decay.

Approximation of the dependence given by Eq. (9) to the measured time-dependent emission allows us to infer the effective deexcitation rate of the level under consideration and the pertaining heavy-particle excitation. The height of the peak intensity, after electron-impact excitation of the level under consideration, is used to perform a normalization. Figure 3 shows the result of such a fit procedure for the emission of the $2p_2$ level of krypton.

The measurement of effective decay rates at various hydrogen partial pressures allows us to determine the quenching coefficient of the observed level with molecular hydrogen from the slope in a so-called Stern-Volmer plot, since the degrees of dissociation (10^{-2}) [2,34] and ionization (10^{-6}) [35,36] are comparatively low in the discharge investigated. Self-quenching of small ($<10\%$) noble-gas admixtures are disregarded because the coefficients are, in general, about one order of magnitude smaller than the quenching coefficients with molecular hydrogen [19–21]. Furthermore, the density of admixtures is kept constant—thus only the measured natural lifetime would be influenced by self-quenching. The natural lifetime can be determined from the axis intercept of the Stern-Volmer plot at zero molecular-hydrogen pressure. Since the natural lifetime of the observed level is usually known from literature, this result is a good check for measurements of levels with unknown quenching coefficients.

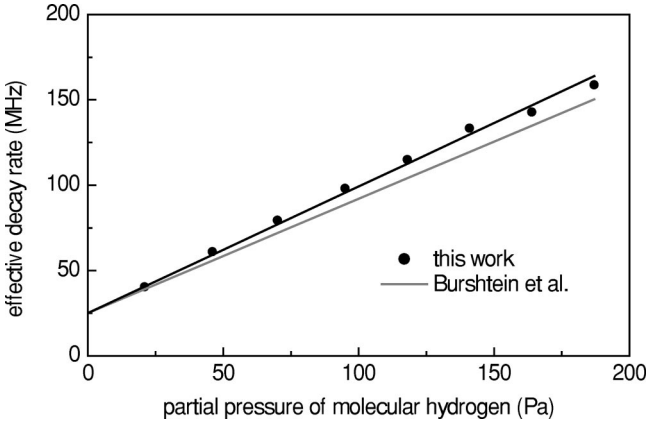

FIG. 5. Stern-Volmer plot of the Fulcher-α ($v=2,N=1$) level.

The gas temperature has to be known for the determination of the density of the collision partner gas from its partial pressure. Its knowledge is also necessary to apply collisional deexcitation coefficients published in the literature because of their temperature dependence [Eq. (2)]. The gas temperature was determined as a function of the pressure in the chamber and of the distance to the grounded electrode at a power of 100 W. The PROES of the Fulcher bands of molecular hydrogen was applied for this purpose [1]. A slight temperature increase has been observed in the pressure range between $p=20$ Pa and $p=190$ Pa, which is relevant for the determination of the deexcitation rates. In view of the measurement error, which can be estimated from the scattering of the measurement points, it is justified to neglect this slight change, and to assume a value of $T=400$ K throughout.

IV. RESULTS

A. Validation on known quenching coefficients

The method described can be validated by measuring and comparing quenching coefficients for the Fulcher-α ($3p\,^3\Pi_u^-, v=2, N=1$), the krypton $2p_2$ and the argon $2p_1$ states, respectively, since these have been determined earlier already with conventional methods [19–21,38].

Investigations with respect to the determination of gas temperatures [1] have shown that cascade processes are responsible for about 8% of the population of the upper Fulcher level—in a good agreement with electron-beam results [37]. This experiment also yields a lifetime for the cascade contributions of 143 ns. Burshtein *et al.* [38] have determined a natural lifetime of 40 ns for the Fulcher level of interest and found a collisional deexcitation coefficient of 45×10^{-10} cm^3 s^{-1} at a gas temperature of 600 K, also in an electron-beam experiment. This yields, according to Eq. (2), a collisional deexcitation coefficient of 37×10^{-10} cm^3 s^{-1} at 400 K. We assume for the effective cascade level the same deexcitation coefficient. This has, however, only very little

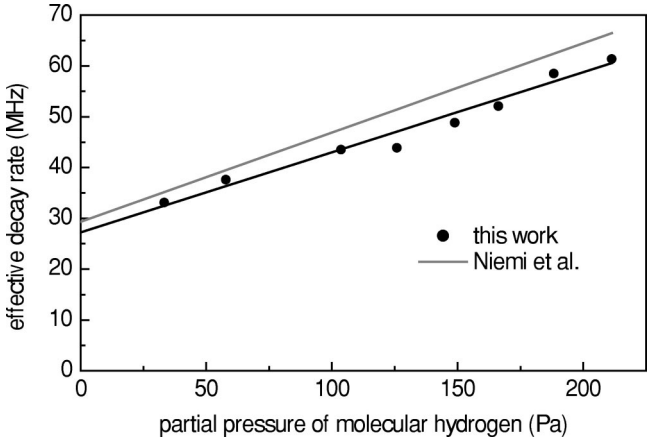

FIG. 6. Stern-Volmer plot of the krypton $2p_2$ state.

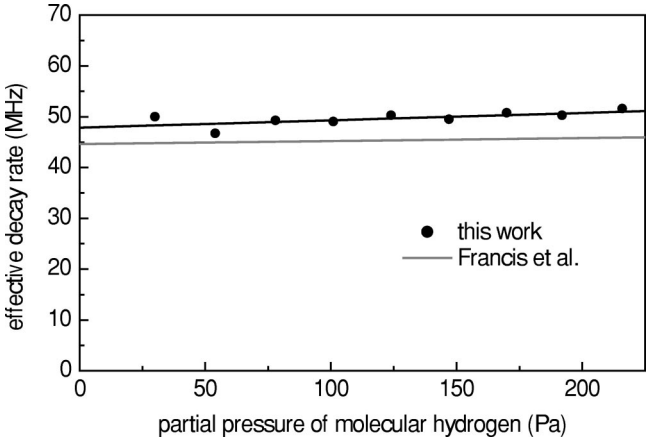

FIG. 7. Stern-Volmer plot of the argon $2p_1$ states.

influence on the result. Figure 5 shows a Stern-Volmer plot with these values taken from the literature and the measured data from the PROES. We obtain with these data a natural lifetime of 40 ± 1 ns and a collisional deexcitation coefficient of $(41\pm1)\times10^{-10}$ cm^3 s^{-1}, both in agreement with literature. The uncertainty given corresponds to the possible error in the linear approximation in the Stern-Volmer plot. The total error that is, in general, clearly higher in view of the approximations made in connection with the determination of the effective deexcitation rates amounts in this case to only about 10% because of the relatively small influence of the cascade contributions.

Chilton *et al.* [31] measured a cascade contribution of $(C/D)_{EB}\approx0.2$ for the krypton $2p_2$ level. This contribution results mainly from the $2s_2$ level. No information was found in the literature for this level, so that typical values were assumed for the collisional deexcitation coefficient and the lifetime—10×10^{-10} cm^3 s^{-1} and 100 ns, respectively. We applied these values as well for other levels, where no detailed information was available. The transition to the ground state was assumed as optically thick in view of the relatively large ground-state density. Niemi *et al.* measured a natural lifetime of 34.1 ns and a collisional deexcitation coefficient of 8.4×10^{-10} cm^3 s^{-1} at 300 K for the krypton $2p_2$ level. This corresponds, according to Eq. (2), to a collisional deexcitation coefficient of 9.7×10^{-10} cm^3 s^{-1} at 400 K. Figure 6 shows a Stern-Volmer-Plot with these literature values and the data obtained by the PROES. A natural lifetime of (36.7 ± 2.1) ns and a collisional deexcitation coefficient of $(8.7\pm0.6)\times10^{-10}$ cm^3 s^{-1} result from these data at a gas temperature at 400 K in a good agreement with the laser experiment. The estimated total error is slightly higher in view of the higher (but still moderate) cascade contribution in comparison to the Fulcher-α level and amounts to $\approx15\%$.

For the argon $2p_1$ level, Chilton *et al.* [29] measured a cascade contribution of $(C/D)_{EB}\approx0.2$, which results mainly from the $3s_1'$ level. Transitions to the ground state can be neglected in this case in view of the very small escape factor of (10^{-5}), so that for the $3s_1'$ level, a lifetime of 56.8 ns results [39]. A lifetime of 22.4 ns can be found in the literature [39] for the investigated $2p_1$ level. The collisional deexcitation coefficient has a very small value of 0.27×10^{-10} cm^3 s^{-1} as determined by Francis *et al.* in a laser experiment at a gas temperature of 300 K. This corresponds to a value of 0.32×10^{-10} cm^3 s^{-1} at 400 K. These literature data are displayed in a Stern-Volmer plot, together with the data from the PROES (Fig. 7). We find for the natural lifetime a value of (20.9 ± 0.4) ns—in a good agreement with literature data. The very small collisional deexcitation coefficient can only be determined with difficulties in the pressure range investigated so that the value of $(0.8\pm0.3)\times10^{-10}$ cm^3 s^{-1} at 400 K can, however, be considered as an upper limit—in good agreement with the laser experiment.

These comparisons with known data from literature demonstrate that the PROES in the sheath region of a CCRF discharge in hydrogen respresents a reliable method to determine collisional deexcitation coefficients [27] with molecular hydrogen. The method is not limited, as already mentioned, by optical selection rules and gives access to high-lying states, e.g., of helium or neon. We will discuss in the following paragraph its application to determine collisional deexcitation coefficients that have not been determined so far.

B. Determination of unknown quenching coefficients

1. Helium

Determination of collisional deexcitation coefficients for helium states ($3\,^1S$,$4\,^1S$,$3\,^3S$,$3\,^3P$,$4\,^3S$) with laser techniques is presently not possible, since the energy differences (20–24 eV) between the ground state and the levels under consideration are too large to allow direct laser excitation from the ground state into $3\,^1S$ and $4\,^1S$, and the triplet states are spin forbidden for optical excitation. Several reasons are in favor of the method of the PROES. One reason is that for all levels, the contributions by cascading transitions are small—$(C/D)_{EB}<0.2$ [40]—so that the lack of information on reliable data for the cascade transitions has no important influence. A second reason is that lifetimes of the states under consideration are comparatively long (37–98 ns) [39]. This leads to a large population density in the interval of

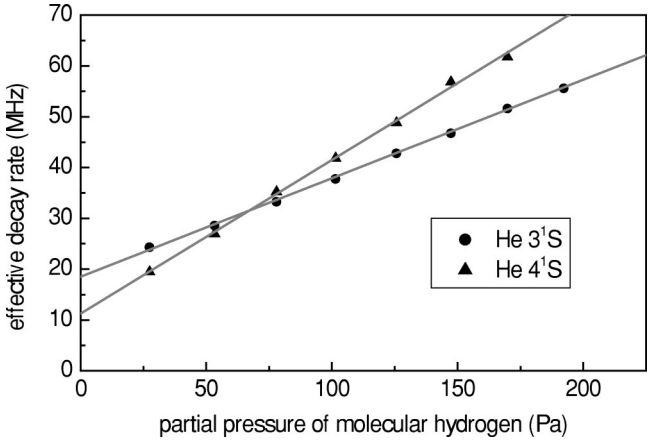

FIG. 8. Stern-Volmer plot of the singlet states $3\,^1S$ and $4\,^1S$ of helium.

observation after the electron-impact excitation, since the builtup population density decays only slowly. The influence of additional population by heavy-particle collisions is accordingly small. The comparatively small intensities connected with the small values of the electron-impact excitation cross sections and small transition rates can be overcome, since helium can be admitted in relatively large quantities ($\approx 10\%$) to the hydrogen discharges without influencing important properties, such as the field reversal phenomenon, on which this method is based.

The cascade contributions [40] and the lifetimes can be taken from the literature [39]. Stern-Volmer plots of the investigated singlet and triplet states are respresented in Figs. 8 and 9. The collisional deexcitation coefficients determined from the slopes are listed in Table I, together with the lifetimes determined from the ordinate intersections and the data published in the literature. In all cases, a very good agreement of the lifetime with the literature values is observed. The error given corresponds to the possible error of the linear approximation in the Stern-Volmer plot. In view of the favorable conditions, we estimate the total error to be not larger than 10%. Included in Table I are also the results for

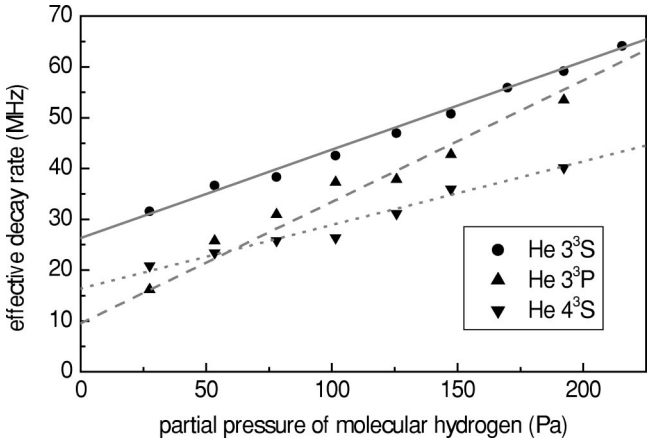

FIG. 9. Stern-Volmer plot of the triplet states $3\,^3S$, $3\,^3P$, and $4\,^3S$ of helium.

TABLE I. Table of the collisional deexcitation coefficients determined with the method outlined above. Also shown are measured lifetimes together with corresponding literature values. The errors given are purely statistical. Systematic errors are discussed in the text. Values in brackets are afflicted by comparatively large systematic errors. The lifetime designated with (*) refers to the case of complete reabsorption of the radiation emitted in transitions down to the ground state. The lifetime indicated with (+) is the lifetime of the Ar $3d_3$ level.

Atomic state	τ_{lit} (ns)	τ (ns)	k_{H_2} (10^{-10} cm^3 s^{-1})
He $3\,^1S$	52	54±1	10.7±0.1
He $4\,^1S$	89	89±5	16.7±0.3
He $3\,^3S$	37	38±1	9.6±0.3
He $3\,^3P$	98	105±9	13.2±0.5
He $4\,^3S$	63	61±3	6.9±0.3
Ne $2p_1$	15	15±1	2.3±0.7
Ne $2p_2$	18	(20±1)	(14.1±0.8)
Ne $2p_4$	19	20±1	12.9±1.2
Ne $2p_6$	22	24±1	7.4±1.2
Kr $2p_1$	(20)	26±1	6.6±0.7
Kr $2p_5$	(20)	22±1	1.7±0.5
$H_2 3s\,^3\Sigma(v=1)$	17		(41±5.0)
$H_2 3p\,^3\Sigma(v=1)$	44		(32±2.0)
Ar $3d_2$	62*	60±9	27.5±1.0
Ar $3d_4$	90	91±24	24.3±1.5
Ar ($3d_1'$and $3d_3$)	121$^+$	115±34	19.6±1.0

Ne, Kr, H_2, and Ar, which are discussed in the following sections.

2. Neon

For the neon levels ($2p_1$,$2p_2$,$2p_4$,$2p_6$) in the energy range of 17–21 eV, a similar situation as for helium applies. The PROES measurements are, however, clearly more difficult in this case because of larger cascade contributions $(C/D)_{EB}<0.4$ [32] and, most important, the much smaller lifetimes (14.5–21.9 ns) [39], since this leads to smaller population densities in the observed interval after the

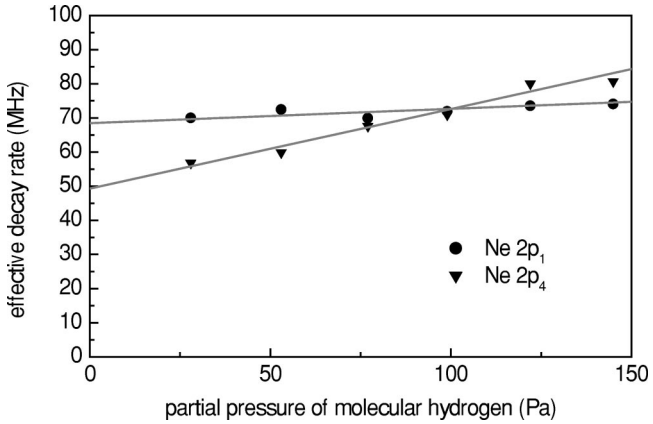

FIG. 10. Stern-Volmer plot of the $2p_1$ and $2p_4$ states of neon.

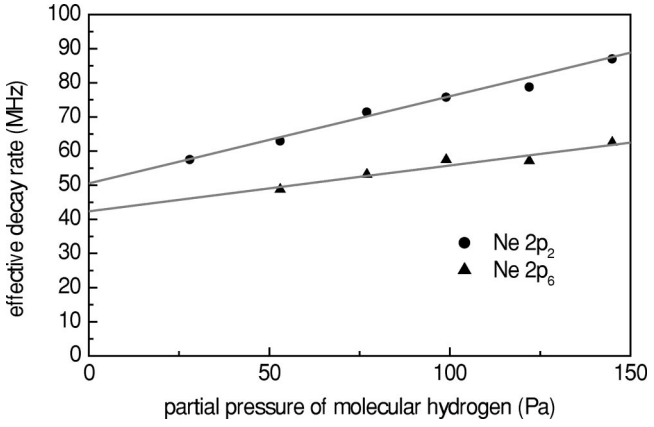

FIG. 11. Stern-Volmer plot of the $2p_2$ and $2p_6$ states of neon.

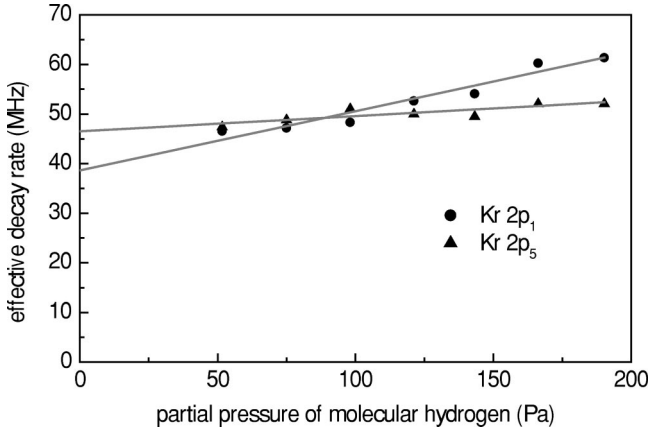

FIG. 12. Stern-Volmer plot of the $2p_1$ and $2p_5$ states of krypton.

electron-impact excitation. The relative importance of the additional heavy-particle excitation increases, therefore, significantly. The cascade contributions [32] and lifetimes [39], on the basis of which the collisional deexcitation coefficients are determined can be found in the literature, whereby transitions of the cascade levels into the ground state are completely reabsorbed. Pertinent Stern-Volmer plots of the neon states investigated are shown in Figs. 10 and 11. A good agreement of the lifetimes with the literature data is obtained using the literature values for the cascade contribution except for the $2p_2$ level. Since the lifetimes for neon are very well known, the cascade contribution for the $2p_2$ level was varied in this case. A cascade contribution of $(C/D)_{EB} \approx 0.9$ is necessary instead of the value given in the literature of $(C/D)_{EB}=0.3$ to result in a lifetime with a reasonable agreement with literature. Two possible explanations exist for the increased cascade contribution in comparison to the literature data: Excitation energy transfer collisions seem likely for the thermal energy of 0.035 eV (400 K) for the relatively close $2p$ levels of neon at the comparatively high partial pressure of several pascals. The $2p_2$ level is located at 18.726 38 eV, whereas the $2p_3$, $2p_4$, $2p_5$ levels are at 18.711 38 eV, 18.704 07 eV, and 18.693 36 eV, so that excitation transfer to the $2p_2$ level is posssible. This is specially true for the $2p_4$ level since its electron-impact excitation cross section is clearly larger than the values for the $2p_2$, $2p_3$, and $2p_5$ levels [32], resulting in a larger population density. A second possibility consists in an excitation transfer to the dominant cascade level $2s_2$ so that an increased cascade contribution would be observed. In view of these uncertainties with the $2p_2$ level, which would lead to a measurement uncertainty of 50%, the results concerning this level are given in brackets in Table I.

The collisional deexcitation coefficients of the remaining neon levels can be determined within an accuracy of about 20%. It is interesting to note that the neon level $2p_1$ plays a unique role as does the argon $2p_1$ level, since the collisional deexcitation coefficients are clearly smaller than those of the other corresponding $2p$ levels.

3. Krypton

Although the krypton $2p$ levels are accessible to two-photon excitation with lasers [19], if optical selection rules allow, only the level $2p_2$ was investigated with molecular hydrogen as a collision partner (to the best of our knowledge). We have, therefore, investigated $2p_1$ and $2p_5$ levels with the PROES, whose cascade contributions—together with the $2p_2$ level—are the smallest $(C/D)_{EB}<0.3$ [31]. The lifetimes of the cascade states are unknown as already mentioned so that we assume a typical lifetime of 100 ns. Stern-Volmer plots of the investigated krypton states are displayed in Fig. 12. The values given in Table I are considered to be reliable within 20%. The resulting longer lifetime of the $2p_1$ level as compared to the literature data [39,41] is not surprising because also in connection with the $2p_2$ level, we have found—in agreement with recent laser measurement [19]—similar deviations with respect to the same reference. The collisional deexcitation coefficient of the $2p_5$ level being clearly smaller than those of $2p_1$ and $2p_2$ levels is remarkable. In contrast to neon and argon, where the respective $2p_1$ level plays a particular role having clearly smaller collisional deexcitation coefficients, this role is played by the $2p_5$ level in the case of krypton. Besides the fact that all these states have a total angular momentum of $J=0$, they are all isolated in the energy-level scheme. This is not the case for the krypton $2p_1$ level.

4. Hydrogen molecule

In the case of the hydrogen molecule, collisional deexcitation coefficients are only known for the already discussed Fulcher-α level. We will discuss in the following, collisional deexcitation coefficients of other levels in order to provide a broader data basis that will also allow us to use other emission lines of molecular hydrogen for diagnostic purposes. The level $3p\,^3\Sigma(v=1)$ is particularly suitable in this context because of its comparatively longer lifetime of 44 ns [42] leading to sufficient population densities in the time interval under investigation. The measurement of this emission line is aggravated, however, because of its small intensity. The lifetime of the $3s\,^3\Sigma(v=1)$ level amounting to 17 ns [43] is comparatively shorter, the corresponding spectral emission is, however, spectrally well isolated. The measurement is, nevertheless, also complicated in this case because the intensity decays considerably below the maximum value after the

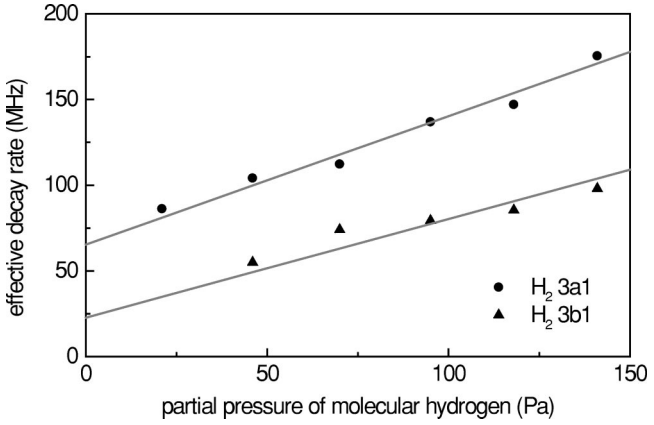

FIG. 13. Stern-Volmer plot of the $3s\,^3\Sigma(v=1)[3a1]$ and $3p\,^3\Sigma(v=1)[3b1]$ states of molecular hydrogen.

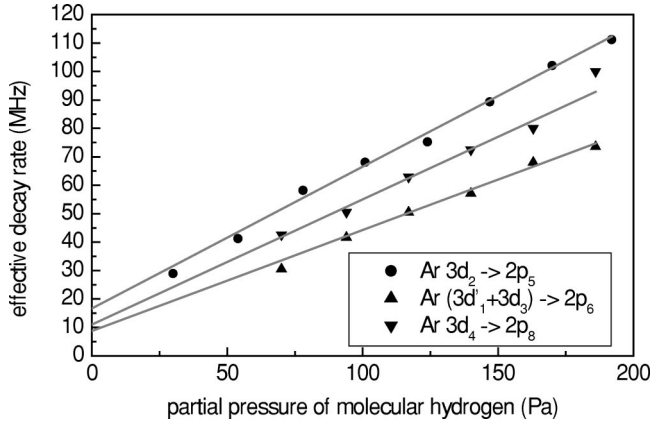

FIG. 14. Stern-Volmer plot of the cascade states $3d_2$, $3d_4$ and $(3d_1'+3d_3)$ of argon.

electron collisional excitation during the interval of observation due to the short lifetime. Cascading contributions for the Fulcher-α level are only minor as already mentioned [1]. We will assume this also for the levels considered here as a first approximation and will, therefore, disregard cascade processes for the determination of collisional deexcitation. The resulting Stern-Volmer plots of the investigated molecular-hydrogen states are represented in Fig. 13. The transitions $3p\,^3\Sigma(v=1,N=2)\rightarrow 2p\,^3\Pi(v=0,N=3)$ and $3s\,^3\Sigma(v=1,N=2)\rightarrow 2p\,^3\Pi(v=1,N=3)$ have been measured. The uncertainties of the inferred effective deexcitation rates are comparably larger due to the small signals. Therefore, lifetime values found in literature have been used as decay rates at zero pressure to determine the collisional deexcitation coefficients. The total error of the collisional deexcitation coefficients is estimated to be of the order of 30% in view of the difficulties mentioned. The collisional deexcitation coefficient of the $3s\,^3\Sigma(v=1)$ level is almost identical with the value found for the Fulcher-α level. The deviation of the $3p\,^3\Sigma(v=1)$ level is within the experimental error.

C. Argon cascade levels

The collisional deexcitation coefficients of the argon $2p$ levels are known from detailed laser spectroscopic investigations [20,21]. On the basis of these data, the PROES allows a determination of the collisional deexcitation coefficients of cascade levels for the case of the $2p_5$, $2p_6$, and $2p_8$ levels that are relatively strongly populated by cascading processes $(C/D)_{EB}\approx 1$ [29]. The emission from these cascade levels is in the infrared, so that a direct measurement is not straightforward. Cascading processes to the $2p_5$ levels result mainly from the $3d_2$ level, and those to the $2p_8$ levels from the $3d_4$ level [29]. The $2p_6$ level population by cascades originates to equal fractions from the $3d_1'$ and $3d_3$ levels [29], so that these can be treated as one effective cascade level. The lifetimes of the $3d_2$ (62 ns) and $3d_4$ (90 ns) levels are found in the literature [39]; it is assumed for the case of the $3d_2$ level that the radiation down to the ground state is completely reabsorbed. Since the lifetime of the $3d_1'$ level is unknown, a lifetime corresponding to the $3d_3$ level (121 ns) is assumed for the effective cascade level of the $2p_6$ level. Stern-Volmer plots of the argon cascade states are represented in Fig. 14. The values determined in this way are estimated to be correct within 30% in view of the indirect character of this method.

V. CONCLUSIONS

Quenching coefficients of noble-gas states with molecular hydrogen as well as self-quenching coefficients of molecular-hydrogen states have been determined by phase-resolved optical emission spectroscopy (PROES) at a capacitively coupled hydrogen rf discharge. The method based on excitation by electron impact takes advantage of the field reversal phase in this type of discharge and is thus not limited by optical selection rules. A comparison of this method with data found in different ways (if those are available) yield a very good agreement in all cases [Fulcher-α $(3p\,^3\Pi_u^-, v=2,N=1)$, krypton $2p_2$, argon $2p_1$]. A number of helium, neon, krypton, and molecular-hydrogen states, to which laser spectroscopic methods have partly no access, have been investigated. Collisional deexcitations of some cascading states of argon have also been determined. The results of the collisional deexcitation coefficients k_{H_2} are summarized, together with measured lifetimes τ and literature data τ_{lit} in Table I.

Possible influences have been discussed where necessary and are included in the measurement error. The data are reliable between 10% and 30%. A good agreement with data published in the literature was also found for cascading contributions in the cases investigated with exception of the neon $2p_2$ state, where a collisional excitation transfer from energetically close states is likely to explain the deviation.

A common behavior for the $2p_1$ levels of neon and argon as well as for the $2p_5$ level of krypton showing clearly smaller collisional deexcitation coefficients than the other respective states was observed and discussed.

The PROES is not necessarily restricted to hydrogen CCRF discharges for the determination of collisional deexcitation coefficients, since similar phenomena are also present in other plasma media of technological relevance. One example is chlorine that has also a pronounced time-

dependent excitation structure including a field reversal phase [44–46]. In recent years, considerable efforts have been made to determine electron collision cross sections that are relevant to the analysis and modeling of discharge plasmas. Due to the vast differences between a single monoenergetic electron collision process and a much more complicated discharge plasma, application of the cross sections for a single process to the latter is not straightforward. The analysis presented in Sec. III of this paper provides a bridge between these two systems and allows us to address the discharge problems in terms of fundamental cross sections.

ACKNOWLEDGMENTS

The authors thank C. Fischer and J. Leistikow for skillful technical assistance and B. Heger (Universität Augsburg) for support in the measurements on molecular-hydrogen states. Support by the ''Deutsche Forschungsgemeinschaft'' in the frame of the Sonderforschungsbereich 191 ''Grundlagen der Niedertemperaturplasmen'' is gratefully acknowledged. One of us (C.C.L.) acknowledges the support by the US Air Force Office of Scientific Research.

[1] T. Gans, V. Schulz-von der Gathen, and H.F. Döbele, Plasma Sources Sci. Technol. **10**, 17 (2001).
[2] V. Schulz-von der Gathen and H.F. Döbele, Plasma Chem. Plasma Process. **16**, 461 (1996).
[3] M.V. Malyshev and V.M. Donnelly, Phys. Rev. E **60**, 6016 (1999).
[4] H.M. Katsch *et al.*, J. Appl. Phys. **88**, 6232 (2000).
[5] A. Goehlich, T. Kawetzki, and H.F. Döbele, J. Chem. Phys. **22**, 9362 (1998).
[6] K. Niemi, V. Schulz-von der Gathen, and H.F. Döbele, J. Phys. D **34**, 2330 (2001).
[7] V. Alekseev and D.W. Setser, J. Phys. Chem. **100**, 5766 (1996).
[8] C.A. Whitehead *et al.*, J. Chem. Phys. **102**, 1965 (1995).
[9] V. Alekseev and D.W. Setser, Chem. Phys. **105**, 4613 (1996).
[10] M.R. Bruce, W.B. Layne, C.A. Whitehead, and J.W. Keto, J. Chem. Phys. **92**, 2917 (1990).
[11] R.S.F. Chang and D.W. Setser, J. Chem. Phys. **69**, 3885 (1978).
[12] W. Demtröder, *Laser Spectroscopy, Basic Concepts and Instrumentation*, 3rd ed. (Springer-Verlag, Berlin, 2000).
[13] J.E. Velazco, J.H. Kolts, and D.W. Setser, J. Chem. Phys. **69**, 4357 (1978).
[14] D.W. Setser, *Book of papers of APP Spring Meeting* (Arbeitsgemeinschaft Plasmaphysik, Bochum, Germany, 2001), p. 49.
[15] M.B. Faist and R.B. Bernstein, J. Chem. Phys. **64**, 2971 (1976).
[16] M.B. Faist and R.B. Bernstein, J. Chem. Phys. **64**, 3924 (1976).
[17] M.J. Wouters, J. Khachan, I.S. Falconer, and B.W. James, J. Phys. B **32**, 2869 (1999).
[18] K.D. Bonin and T.J. McIlrath, J. Mod. Opt. Soc. Am. B **1**, 52 (1984).
[19] K. Niemi, V. Schulz–von der Gathen, and H.F. Döbele, in *Proceedings of the Seventh International Conference on Hakone, Greifswald*, edited by H.E. Wagner, J.F. Behnke, and A. Babucké (Universität Greifswald, Greifswald, Germany, 2000), p. 199.
[20] A. Francis, U. Czarnetzki, H.F. Döbele, and N. Sadeghi, Appl. Phys. Lett. **71**, 3796 (1997).
[21] A. Francis, U. Czarnetzki, H.F. Döbele, and N. Sadeghi, Eur. Phys. J.: Appl. Phys. **4**, 239 (1998).
[22] R.S.F. Chang and D.W. Setser, J. Chem. Phys. **72**, 4099 (1980).
[23] H.M. Katsch, E. Quandt, and Th. Schneider, Plasma Phys. Controlled Fusion **38**, 183 (1996).
[24] T. Gans, V. Schulz-von der Gathen, U. Czarnetzki, and H.F. Döbele, Contrib. Plasma Phys. **42**, 596 (2002).
[25] U. Czarnetzki, D. Luggenhölscher, and H.F. Döbele, Plasma Sources Sci. Technol. **8**, 230 (1999).
[26] U. Czarnetzki, D. Luggenhölscher, and H.F. Döbele, Appl. Phys. A: Mater. Sci. Process. **72**, 509 (2001).
[27] T. Gans, Chun C. Lin, V. Schulz–von der Gathen, and H.F. Döbele, J. Phys. D: Appl. Phys. **34**, L1 (2001).
[28] J.E. Chilton, M.D. Stewart, Jr., and C.C. Lin, Phys. Rev. A **62**, 32714 (2000).
[29] J.E. Chilton, J.B. Boffard, R.S. Schappe, and C.C. Lin, Phys. Rev. A **57**, 267 (1998).
[30] J.E. Chilton and C.C. Lin, Phys. Rev. A **60**, 3712 (1999).
[31] J.E. Chilton, M.D. Stewart, Jr., and C.C. Lin, Phys. Rev. A **62**, 32714 (2000).
[32] J.E. Chilton, M.D. Stewart, Jr., and C.C. Lin, Phys. Rev. A **61**, 52708 (2000).
[33] J.T. Fons and C.C. Lin, Phys. Rev. A **58**, 4603 (1998).
[34] L. Chérigier, U. Czarnetzki, D. Luggenhölscher, V. Schulz–von der Gathen, and H.F. Döbele, J. Appl. Phys. **85**, 696 (1999).
[35] C. Lukas, M. Müller, V. Schulz–von der Gathen, and H.F. Döbele, Plasma Sources Sci. Technol. **1**, 106 (1999).
[36] C.M.O. Mahony, J. McFarland, P.G. Steen, and W.G. Graham, Appl. Phys. Lett. **75**, 331 (1999).
[37] R.L. Day and R.J. Anderson, J. Chem. Phys. **69**, 5518 (1978).
[38] M.L. Burshtein *et al.*, Opt. Spectrosc. **68**, 166 (1990).
[39] See NIST atomic spectra database http://physlab.nist.gov/cgi-bin/AtData/main_asd.
[40] R.M. St. John, F.L. Miller, and Chun C. Lin, Phys. Rev. **134**, A888 (1964).
[41] R.S.F. Chang, H. Horiguchi, and D.W. Setser, J. Chem. Phys. **73**, 778 (1980).
[42] S.A. Astashkevich *et al.*, J. Quant. Spectrosc. Radiat. Transf. **56**, 725 (1996)
[43] E.E. Eyler and F.M. Pipkin, Phys. Rev. Lett. **47**, 1270 (1981)
[44] O. Leroy, P. Stratil, J. Perrin, J. Jolly, and P. Belenguer, J. Phys. D: Appl. Phys. **28**, 500 (1995).
[45] D.L. Flamm and J. Donnelly, J. Appl. Phys. **59**, 1052 (1986).
[46] E. Gogolides, J.P. Nicolai, and H.H. Sawin, J. Vac. Sci. Technol. A **7**, 1001 (1989).